A&A 529, A122 (2011)
DOI: 10.1051/0004-6361/201014221

Astronomy & Astrophysics

AKARI detections of hot dust in luminous infrared galaxies

Search for dusty active galactic nuclei

S. Oyabu[1], D. Ishihara[1], M. Malkan[2], H. Matsuhara[3], T. Wada[3], T. Nakagawa[3], Y. Ohyama[4], Y. Toba[3,5], T. Onaka[6], S. Takita[3], H. Kataza[3], I. Yamamura[3], and M. Shirahata[3]

[1] Graduate School of Science, Nagoya University, Furo-cho, Chikusa-ku, Nagoya, Aichi 464-8602, Japan
e-mail: oyabu@u.phys.nagoya-u.ac.jp
[2] Department of Physics and Astronomy, University of California, Los Angeles, CA 90095-1547, USA
[3] Institute of Space and Astronautical Science, Japan Aerospace Exploration Agency, 3-1-1 Yosinodai, Chuo-ku, Sagamihara, Kanagawa, 252-5210, Japan
[4] Academia Sinica, Institute of Astronomy and Astrophysics, Taiwan
[5] Department of Space and Astronautical Science, the Graduate University for Advanced Studies (Sokendai), 3-1-1 Yoshinodai, Chuo-ku, Sagamihara, Kanagawa, 252-5210, Japan
[6] Department of Astronomy, University of Tokyo, 7-3-1 Hongo, Bunkyo-ku, Tokyo, 113-0033, Japan

Received 9 February 2010 / Accepted 4 March 2011

ABSTRACT

Aims. We present a new sample of active galactic nuclei (AGNs) identified using the catalog of the AKARI Mid-infrared (MIR) All-Sky Survey. Our MIR search has the advantage of detecting AGNs that are obscured at optical wavelengths by extinction.
Methods. We first selected AKARI 9 μm excess sources with $F(9\ \mu\mathrm{m})/F(K_\mathrm{S}) > 2$ where K_S magnitudes were taken from the Two Micron All Sky Survey. We then obtained follow-up near-infrared spectroscopy with the AKARI/IRC to confirm that the excess is caused by hot dust. We also obtained optical spectroscopy with the Kast Double Spectrograph on the Shane 3-m telescope at Lick Observatory.
Results. On the basis of these observations, we detected hot dust with a characteristic temperature of $\gtrsim$500 K in two luminous infrared galaxies. The hot dust is suspected to be associated with AGNs that exhibit their nonstellar activity not in the optical, but in the near- and mid-infrared bands, i.e., they harbor buried AGNs. The host galaxy stellar masses of $\sim 4-6 \times 10^9\ M_\odot$ are small compared with the hosts in optically-selected AGN populations. These objects were missed by previous surveys, demonstrating the power of the AKARI MIR All-Sky Survey to widen AGN searches to include more heavily obscured objects. The existence of multiple dusty star clusters with massive stars cannot be completely ruled out with our current data.

Key words. galaxies: active – galaxies: nuclei – infrared: galaxies

1. Introduction

Many observations have found evidence of the presence of a large number of heavily obscured active galactic nuclei (AGNs). It is found that a significant number of ultra-luminous infrared galaxies contain AGNs at their centers (e.g. Sanders & Mirabel 1996; Lutz et al. 1998; Imanishi et al. 2008). Various hard X-ray and soft gamma-ray observations (Maiolino et al. 1998; Risaliti et al. 1999; Malizia et al. 2009) indicate that about 80 percent of the AGNs in the local Universe are obscured. AGN synthesis models of the X-ray background postulate their existence in order to explain the flat spectrum of the hard X-ray background (e.g. Ueda et al. 2003). These black holes contribute to the local black hole mass density (Fabian & Iwasawa 1999), and are potentially important contributors to the growth of supermassive black holes throughout the history of the universe. However, the nature of this population, even in the local universe, is only poorly understood, because of the strong selection bias against finding them at optical wavelengths.

Mid-infrared (MIR) AGN searches can overcome this obstacle by penetrating through dust extinction to identify most of the AGN population,including Type 2 Seyferts and buried AGNs. The original IRAS 12 μm active galaxy samples (Spinoglio & Malkan 1989; Rush et al. 1993) provide an unbiased sample of local active galaxies. Using the ISOCAM parallel mode survey of 10 square degrees at 6.7 μm (LW2), Leipski et al. (2005, 2007) succeeded in finding redder Type 1 AGNs as well as Type 2's. Several searches have also been performed using the near- and mid-infrared bands in the *Spitzer* Space Telescope (e.g. Lacy et al. 2004; Alonso-Herrero et al. 2006; Polletta et al. 2006).

AKARI performed an all-sky survey at 9 and 18 μm as well as at four far-infrared (FIR) bands (65, 90, 140, and 160 μm). It provided improvements of about one order of magnitude compared to that of IRAS in both spatial resolution and sensitivity in the mid-infrared bands. The details of the survey are described in Ishihara et al. (2010).

In this paper, we present the first results of our search for AGNs based on this AKARI MIR All-Sky Survey. We discovered two galaxies LEDA 84274 and IRAS 01250+2832, which have a compact hot $\gtrsim$500 K dust component. The hot dust component may be heated by the central engine of the AGN, even though their optical spectra do not show any AGN characteristics.

The observations, data reduction, and results are described in Sect. 2. In Sect. 3, we describe the multiwavelength properties of the two galaxies and in Sect. 4 the hot dust components we found in the galaxies are discussed. The discussion is presented in Sect. 5, and a summary is given in Sect. 6. Throughout the paper, we assume a flat cosmology with $\Omega = 0.3$, $\Lambda = 0.7$, and $H_0 = 70\,\mathrm{km\,s^{-1}\,Mpc^{-1}}$.

2. Observations and results

The initial identification of the AKARI MIR All-Sky Survey sources involves association with the Two Micron All Sky Survey (2MASS) catalog (Skrutskie et al. 2006). This search highlights unusually red AKARI MIR sources with $F(9\,\mu\mathrm{m})/F(K_\mathrm{s}) > 2$, at high Galactic latitudes, $|b| > 30°$ after excluding regions around the Large and Small Magellanic Clouds. To examine the origin of the excess of $F(9\,\mu\mathrm{m})/F(K_\mathrm{s}) > 2$, we performed follow-up observations with the AKARI near-infrared (NIR) spectrometer.

Using the AKARI spectra of the 2.5−5 μm wavelength range, AGNs can be distinguished by their red continuum emission, while strong polycyclic aromatic hydrocarbons (PAH) emission is detected in star-forming galaxies. To measure the redshift and search optically for AGN or star-formation signatures, optical spectra were also taken with the Share 3 m telescope at the Lick Observatory.

During these follow-up observations, we discovered two buried AGN candidates that have steep red NIR continuum from hot dust, but do not show any AGN features in optical spectra, such as strong high-ionization emission lines. Table 1 summarizes the properties of our targets, including the fluxes in the AKARI All-Sky MIR and FIR Survey catalogs (Ishihara et al. 2010; Yamamura et al. 2009). LEDA 84274 is identified as the FIR source, IRAS 14416+6618. Previous optical spectroscopy of LEDA 84274 (Kim et al. 1995; Veilleux et al. 1995) reported a low-ionization spectrum with strong Balmer lines, indicating an H II-region-like or star-forming galaxy at $z = 0.0377$. Thus, the gas emitting these optical lines is photoionized by early-type stars. For IRAS 01250+2832, this is its first reported identification as a galaxy at $z = 0.043$.

Table 1. Data for LEDA 84274 and IRAS 01250+2832.

Property	LEDA 84274	IRAS 01250+2832
RA(J2000)[a]	14 42 34.88	01 27 53.95
Dec(J2000)[a]	+66 06 04.3	+28 47 51.0
Redshift	0.0377	0.043
J(mag)[b]	13.756 ± 0.054	14.774 ± 0.117
H(mag)[b]	13.293 ± 0.090	13.941 ± 0.131
K_s(mag)[b]	12.744 ± 0.083	13.462 ± 0.169
IRAS 12 μm (Jy)[c]	0.10 ± 0.03 (2)	<0.11 (1)
IRAS 25 μm (Jy)[c]	0.56 ± 0.03(3)	0.28 ± 0.05(2)
IRAS 60 μm (Jy)[c]	2.19 ± 0.20(3)	0.52 ± 0.03(3)
IRAS 100 μm (Jy)[c]	1.80 ± 0.14(2)	<0.76 (1)
AKARI 9 μm (Jy)[d]	0.084 ± 0.007	0.105 ± 0.010
AKARI 18 μm (Jy)[d]	0.344 ± 0.016	0.182 ± 0.017
AKARI 65 μm (Jy)[e]	1.89 ± 0.22(1)	<3.2[i]
AKARI 90 μm (Jy)[e]	1.51 ± 0.04(3)	<0.55[i]
AKARI 140 μm (Jy)[e]	1.79 ± 0.26(1)	<3.8[i]
AKARI 160 μm (Jy)[e]	<7.5[i]	<7.5[i]
$L_\mathrm{IR}(L_\odot)$[f]	1.8×10^{11}	1.0×10^{11}
$L_\mathrm{IR}(L_\odot)$[g]	1.8×10^{11}	0.9×10^{11}
$D_\mathrm{n}(4000)$[h]	1.10 ± 0.02	1.63 ± 0.08

Notes. [a] The 2MASS coordinates. Units of right ascension are hours, minutes, and seconds, and units of declination are degrees, arcminutes, and arcseconds. [b] The 2MASS magnitudes in All-Sky Extended Source Catalog. [c] Fluxes are from the IRAS Faint Source (Moshir et al. 1992). Numbers in parentheses indicate the flux qualities. [d] AKARI/IRC Mid-infrared All-Sky Survey Point Source Catalog Ver. 1 (Ishihara et al. 2010). [e] AKARI/FIS FIR All-Sky Survey Bright Source Catalog Ver. 1 (Yamamura et al. 2009). The number in parentheses indicates the flux qualities. (3) denotes a clear detection, and (1) indicates the flux at the position. [f] The 8−1000 μm infrared luminosity $L_\mathrm{IR} = 4\pi D_\mathrm{L}^2 F_\mathrm{IR}$ is computed using IRAS fluxes, $F_\mathrm{IR} = (1.8\times10^{-14})(13.56 \times F_{12} + 5.26 \times F_{25} + 2.54 \times F_{60} + 1.0 \times F_{100})\,\mathrm{W\,m^{-2}}$ (Kim et al. 1995). We used IRAS upper limits when IRAS did not detect a source. [g] The 8−1000 μm infrared luminosity is derived from the blackbody fits. See Sects. 3.1 and 3.2 for details. [h] $D_\mathrm{n}(4000)$ is the discontinuity of the spectrum around 4000 Å. See Sect. 2.2 for details. [i] Detection limits in Yamamura et al. (2010), which are estimated from the peaks of $\log N - \log S$ plots, corresponding to ∼90 percent completeness.

2.1. AKARI near-infrared spectroscopy

We performed NIR spectroscopy using the InfraRed Camera (IRC) (Onaka et al. 2007; Ohyama et al. 2007) onboard the AKARI satellite (Murakami et al. 2007). We used the IRC channel NIR, which uses a 512×412 InSb array and the astronomical observation template Z4 (AOT Z4) designed for spectroscopy. AOT Z4 replaces the imaging filters by the transmission-type dispersers on the filter wheel to take NIR spectra. The NIR grism (NG) was set to cover the wavelengths of 2.5−5 μm at a resolution of about 100. The $1' \times 1'$ slit was used to avoid any overlap with other sources.

AKARI NIR spectra were obtained during December 2008−July 2009. The total exposure times for both objects are 792 s. We observed both objects twice in the AKARI warm (Phase3) mission period to correct hot pixels caused by the relatively high temperature (∼40 K) of the detector.

The data were processed using the IRC Phase3 dedicated data reduction package, IRC_SPECRED Ver. 20090211 (Ohyama et al. 2007). Dark subtraction, linearity correction, flat-field correction, and various image anomaly corrections were first performed. Multiple exposures were then coadded. After performing wavelength- and flux-calibration, the spectra of the object were extracted. The aperture size for the spectrum extraction was set to be 3 pixels (4.5″). Aperture corrections were also applied at the end of the processing. The present data reduction gives an uncertainty in wavelength of ∼0.01 μm and the error in the absolute flux is smaller than 20 percent.

Figure 1 shows the calibrated spectra of LEDA 84274 and IRAS 01250+2832. Both objects display steep red continuum. We find emission lines of PAH at 3.3 μm and Brα at 4.05 μm for LEDA 84274. The measured line fluxes are given in Table 2. For IRAS 01250+2832, the R-branch of CO ro-vibrational absorption is detected at 4.75 μm. Upper limits to the fluxes of the PAH bands at 3.3 μm and Brα at 4.05 μm are given in Table 2.

2.2. Lick optical spectroscopy

We performed optical spectroscopy of LEDA 84274 and IRAS 01250+2832 using the Kast Double Spectrograph on the Shane 3-m telescope at the Lick Observatory in 2009 March and August, respectively. This spectrograph has two separate parallel channels – one optimized for the blue and the other for the red. The 600/4310 grism and the 600/7500 grating were used in the blue and red spectrometers, respectively. The wavelength coverage was 3700−8300 Å with a small gap at around 5500 Å

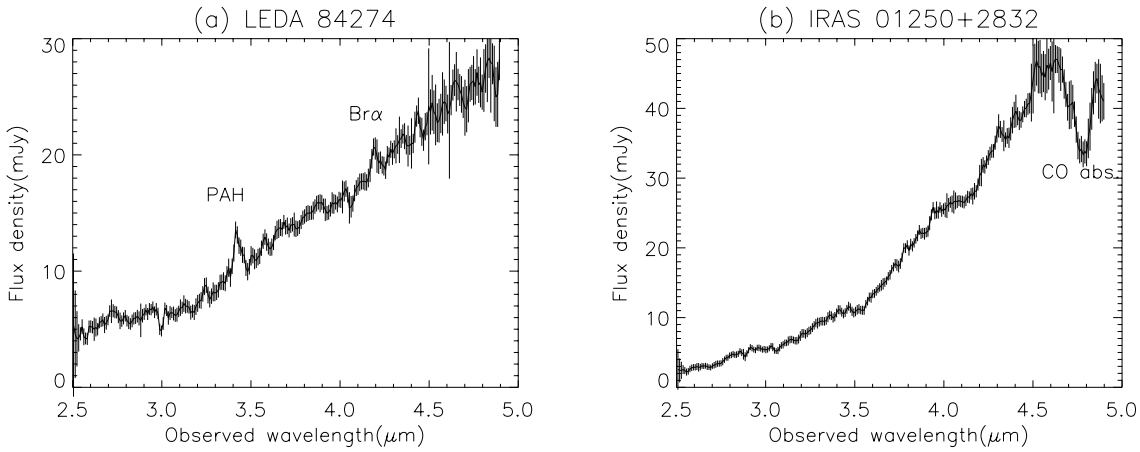

Fig. 1. AKARI NIR spectra of **a)** LEDA 84274 and **b)** IRAS 01250+2832 in the observed wavelength frame. The thin vertical lines represent 1σ errors.

Table 2. AKARI NIR emission features of LEDA 84274 and IRAS 01250+2832.

Name	Obs. wave.[a] (μm)	Flux[b] (10^{-16} erg s^{-1} cm^{-2})	Obs. EW[c] (μm)
LEDA 84274			
PAH 3.3 μm	3.416 ± 0.010	437 ± 30	0.018 ± 0.001
Brα 4.05 μm	4.200 ± 0.010	178 ± 26	0.060 ± 0.009
IRAS 01250 + 2832			
PAH 3.3 μm	...	<75[d]	<0.003[d]
Brα 4.05 μm	...	<100[d]	<0.001[d]

Notes. [(a)] Observed wavelength. [(b)] Line flux and 1σ error in the measurement. [(c)] Observed equivalent width in μm. [(d)] Upper limits (3σ) are estimated with the line widths for LEDA 84274.

Table 3. Optical emission lines of LEDA 84274 and IRAS 01250+2832.

Name	Obs. wave.[a] (Å)	Flux (10^{-16} erg s^{-1} cm^{-2})	Obs. EW[b] (Å)	Ratio with Hα[c] This work	Ratio with Hα[d] Kim et al. (1995)
LEDA 84274					
[O II]	3870	317.0 ± 1.9	54.6 ± 0.3	0.58	0.30
Hγ	4504	46.5 ± 1.4	7.4 ± 0.2	0.08	...
Hβ	5045	120.5 ± 1.1	20.6 ± 0.2	0.22	0.18
[O III]	5146	81.9 ± 1.1	13.5 ± 0.2	0.15	0.12
[O III]	5196	240.0 ± 1.1	40.6 ± 0.2	0.44	0.37
HeI	6094	18.8 ± 0.5	3.2 ± 0.1	0.03	...
[O I]	6536	23.0 ± 0.4	4.4 ± 0.1	0.04	0.04
[O I]	6603	8.5 ± 0.4	1.6 ± 0.1	0.02	...
[N II]	6794	61.1 ± 0.6	11.8 ± 0.1	0.11	0.10
Hα	6808	549.0 ± 0.5	106.1 ± 0.1	1.00	1.00
[N II]	6830	178.0 ± 0.5	34.6 ± 0.1	0.32	0.31
[S II]	6968	78.9 ± 0.4	15.5 ± 0.1	0.14	0.14
[S II]	6983	65.1 ± 0.4	12.8 ± 0.1	0.12	0.11
IRAS 01250+2832					
[N II]	6828	4.3 ± 0.8	1.5 ± 0.3	1.02	...
Hα	6844	4.2 ± 0.8	1.4 ± 0.3	1.00	...
[N II]	6864	12.1 ± 0.8	4.2 ± 0.3	2.88	...

Notes. [(a)] Observed wavelength. A typical error of measurements is less than 1 Å. [(b)] Observed equivalent width. [(c)] Emission line ratio with Hα in this work. A typical measurement error is less than 0.01. [(d)] Emission line ratio with Hα in Kim et al. (1995).

produced by the dichroic beamsplitter. The exposure times for both galaxies were 1500 s.

The spectra of both LEDA 84274 and IRAS 01250+2832 are shown in Fig. 2. We identify the strong emission lines in LEDA 84274 and IRAS 01250+2832 as shown in Table 3. On the basis of these identifications, we determine the redshift of $z = 0.0377$ for LEDA 84274, which is consistent with the redshift previously determined by Kim et al. (1995). The line ratios of the present results are consistent with previous ones, while the emission line flux ratios relative to those of the Hα line in bluer part of the spectra are slightly larger than those in Kim et al. (1995). The spectrum of IRAS 01250+2832 shows a series

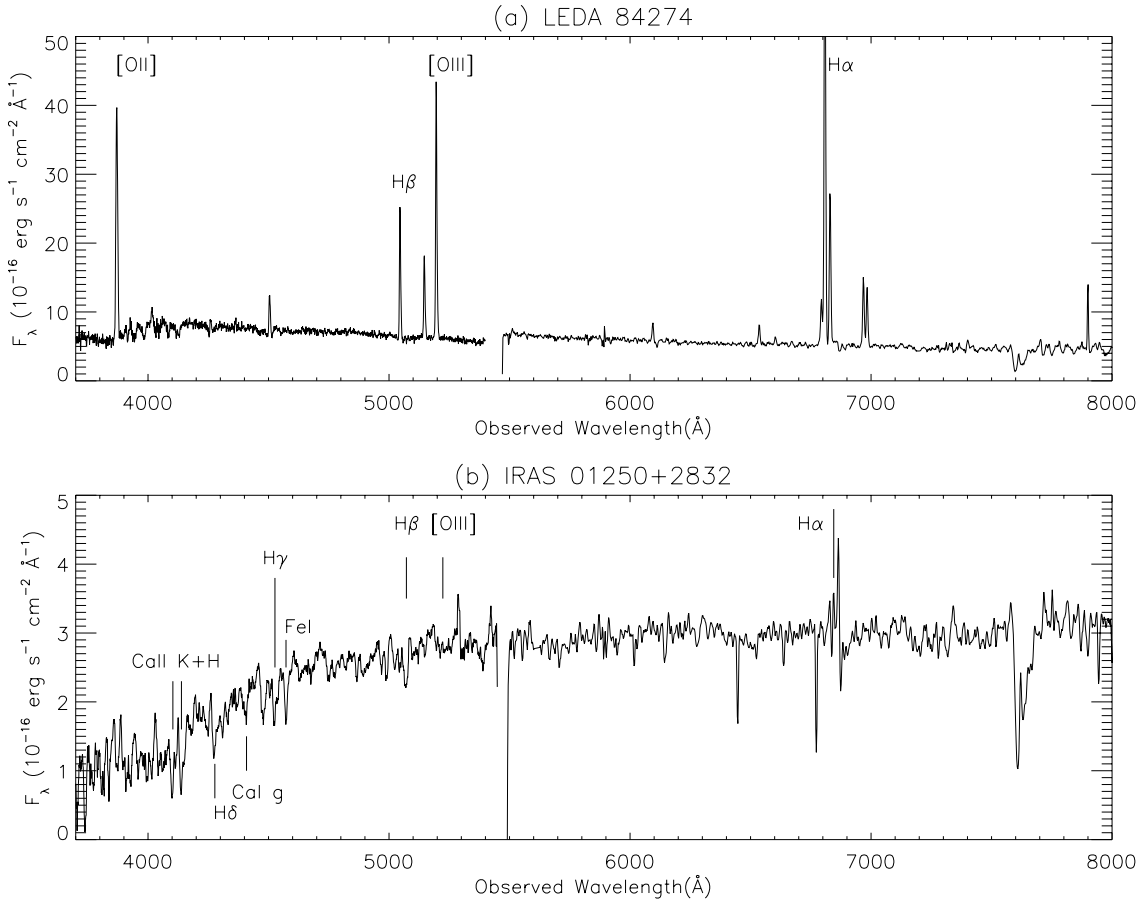

Fig. 2. Optical spectra of **a)** LEDA 84274 and **b)** IRAS 01250+2832. In **b)**, the positions of the Hβ 4861 Å and [O III] 5007 Å lines are indicated.

of absorption lines in the blue part of its spectrum. We identify these absorption lines as Ca II H+K, Hδ, Ca I g-band, Hγ, and Fe I as shown in Fig. 2b. Although Hα 6563 Å and [N II] 6548, 6583 Å emission lines are detected, no other emission lines are detected. We use the absorption lines to estimate the redshift of $z = 0.043$.

To examine the galaxy stellar population, we measure the 4000 Å discontinuity. This discontinuity is originally defined by

$$D(4000) = \frac{\left(\lambda_2^- - \lambda_1^-\right) \int_{\lambda_1^+}^{\lambda_2^+} F\nu \mathrm{d}\lambda}{\left(\lambda_2^+ - \lambda_1^+\right) \int_{\lambda_1^-}^{\lambda_2^-} F\nu \mathrm{d}\lambda}, \quad (1)$$

where $(\lambda_1^-, \lambda_2^-, \lambda_1^+, \lambda_2^+) = (3750, 3950, 4050, 4250)$ Å (Bruzual 1983). A definition using narrower continuum bands $(\lambda_1^-, \lambda_2^-, \lambda_1^+, \lambda_2^+) = (3850, 3950, 4000, 4100)$ was introduced by Balogh et al. (1999) and is widely used. The advantage of the narrower bands is that the index is less sensitive to reddening. We adopt the narrow-band definition, and denote this index as $D_\mathrm{n}(4000)$. The resultant $D_\mathrm{n}(4000)$ indices are 1.10 ± 0.02 and 1.63 ± 0.08 for LEDA 84274 and IRAS 01250+2832, respectively. On the basis of these indices, LEDA 84274 has the spectrum of a late-type galaxy, and IRAS 01250+2832 that of an elliptical galaxy.

3. Multiwavelength properties

The AKARI NIR spectroscopic observations display a steep red continuum in both galaxies, while they have different characteristics in the optical and FIR. The following subsections describe the properties of each galaxy.

3.1. LEDA 84274

The various properties of LEDA 84274 indicate that it currently has a high star-formation rate. The optical emission line ratios such as [N II]6583 Å/Hα vs. [O III]5007 Å/Hβ, [S II]6716 Å+6731 Å/Hα vs. [O III]5007 Å/Hβ, and [O I]6300 Å/Hα vs. [O III]5007 Å/Hβ are in the range of a star-forming galaxy according to Veilleux et al. (1995), who used the spectrum taken by Kim et al. (1995). The PAH emission band detected at 3.416 μm is known to be associated with star-formation activity. FIR detections with IRAS and AKARI are also consistent with a high star-formation rate. The 20 cm flux density in the NRAO VLA Sky Survey (NVSS; Condon et al. 1998) is reported to be 4.2 ± 0.4 mJy. The logarithmic ratio of the FIR to radio continuum flux densities $\log[F_\mathrm{fir}/(3.75 \times 10^{12}\ \mathrm{Hz})/f_\nu(20\ \mathrm{cm})] = 2.7 \pm 0.1$, where F_fir is the flux between 42.5 and 122.5 μm[1] (Helou et al. 1985), is consistent with 2.4 ± 0.2 of the star-formation activity in normal, infrared, and luminous infrared galaxies including ultra-luminous infrared galaxies (Sanders & Mirabel 1996). This relative weakness of radio emission in LEDA 84274 is clearly inconsistent with the ratio (2.1) observed in local Seyfert galaxies (Rush et al. 1996).

Before we estimate the star-formation rate in LEDA 84274, we estimate the amount of reddening in the emission region, based on the Balmer line ratio, Hα/Hβ. The equivalent widths of the Balmer lines are so large that we did not apply any correction for the underlying stellar absorption lines. The result is

[1] $F_\mathrm{fir} = 1.26 \times 10^{-14} \times [2.58 f_\nu(60\ \mu\mathrm{m}) + f_\nu(100\ \mu\mathrm{m})]$ where f_ν are the flux densities in Jy, and F_fir is in W m^{-2}.

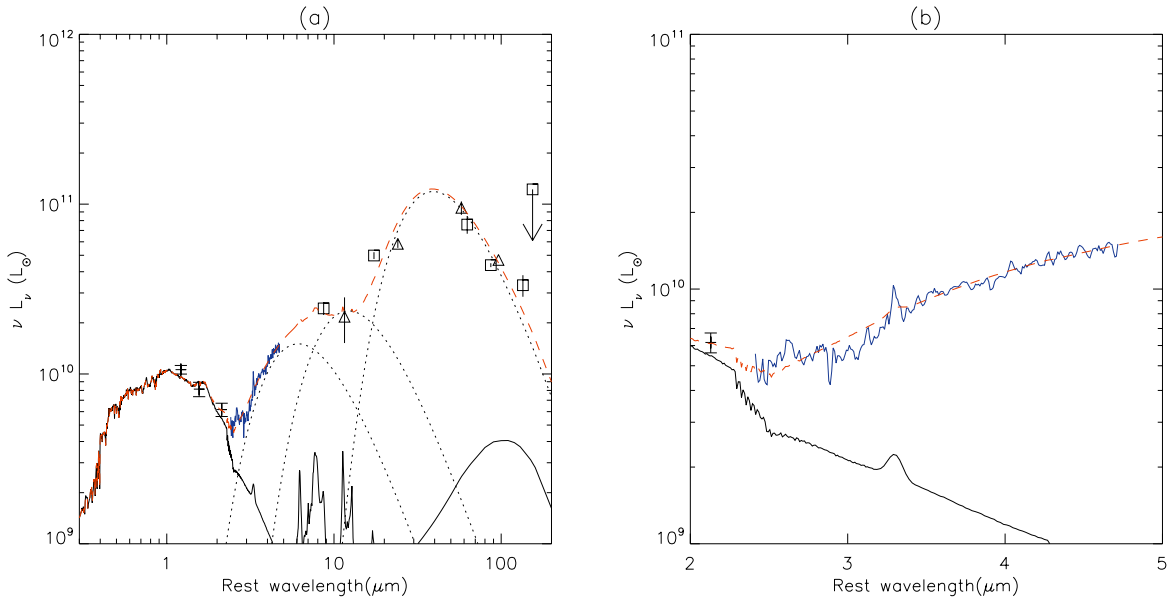

Fig. 3. Spectral energy distribution of **a)** LEDA 84274. The blue line shows the AKARI NIR spectroscopy. Squares and triangles represent the AKARI All-Sky Survey and IRAS, respectively. Crosses show the 2MASS photometry. The solid line (black) is a model template of a Sc galaxy (Polletta et al. 2007). The model line normalized at the 2MASS photometry. A dashed line (red) represents the Sc galaxy template plus three blackbody components, the temperatures of which are 600 K, 300 K, and 93 K. Dotted lines represent each blackbody component. **b)** Close-up of the 2−5 μm range of LEDA 84274, to clearly show the model and the blackbody component with 600 K. See text for details.

$A_V = 1.3$ mag, when we assume case B recombination with $T_e = 10\,000$ K (Osterbrock & Ferland 2006) and the extinction law (Weingartner & Draine 2001), while we get $A_V = 3.5$ mag using the recombination line ratio of Brα/Hα. The difference can be explained by the deeper penetration of Brα photons, suggesting that only the surface of the emitting region contributes to optical emission lines.

We calculate the *SFR* using the PAH 3.3 μm band, which is not expected to be affected by an AGN. With the empirical ratio, $L_{\rm PAH\ 3.3}/L_{\rm IR} \sim 2{-}3 \times 10^{-4}$ for starburst galaxies (Mouri et al. 1990) and the conversion of the IR luminosity into *SFR* (Kennicutt 1998), the *SFR* of LEDA 84274 is estimated to be 20−30 $M_\odot$ year^{-1}. We estimate *SFR*s of 7 and 25 $M_\odot$ year^{-1} using the optical Hα emission line with $A_V = 1.3$ and the NIR Brα emission line with $A_V = 3.5$, respectively. *SFR*(Brα) is consistent with *SFR*(PAH), while *SFR*(Hα) is lower than the others, which can be explained similarly by a highly non-uniform A_V. The infrared luminosity calculated from the IRAS measurement is $L_{\rm IR} = 1.8 \times 10^{11}\ L_\odot$, which corresponds to *SFR*(IR) = 31 $M_\odot$ year^{-1}.

The spectral energy distribution (SED) of LEDA 84274 is presented in Fig. 3. A SED model is also overplotted in Fig. 3a. For LEDA 84274, the Sc galaxy template (Polletta et al. 2007) agrees with the photometric points in the *J*-, *H*-, and K_S-bands. To fit the AKARI NIR spectrum, we assume that the spectrum is a summation of the Sc galaxy template and dust with a single-temperature modified blackbody. The model is defined as

$$F_\lambda = C_1\, F_{\rm galaxy} + C_2\, B_\lambda(T_{\rm dust})\,(1 - \exp(-\tau_\lambda)), \qquad (2)$$

where $F_{\rm galaxy}$ is the Sc galaxy template, $B_\lambda(T_{\rm dust})$ is the Planck function with dust temperature $T_{\rm dust}$ and τ_λ is the dust optical depth. For the frequency dependence of the dust optical depth, we adopt $\tau_\lambda = C_3 \lambda^{-\beta}$. The parameters C_1, C_2, $T_{\rm dust}$, C_3, and β are derived by χ^2 fitting the AKARI NIR spectrum. The fit indicates that 530 K $< T_{\rm dust} <$ 670 K if optically thick, or 470 K $< T_{\rm dust} <$ 580 K if optically thin with $\tau_{1\ \mu{\rm m}} \lesssim 1$ and $\beta = 1{-}2$. Figure 3b shows a close-up of a fit with an optically thick blackbody of $T_{\rm dust} = 600$ K.

In addition, we must add a cool component of dust with $T_{\rm dust} = 93 \pm 5$ K and $\beta = 0$ to explain the IRAS and AKARI photometric data at wavelengths longer than 12 μm. For AKARI 9 μm and IRAS 12 μm data, we need to add one more component of temperature $T_{\rm dust} \sim 300$ K. There is no strong constraint on either the temperature or the emissivity.

The fitting results are shown in Fig. 3a. From the blackbody fits, we derived a total infrared luminosity of $L_{\rm IR} = 1.8 \times 10^{11}\ L_\odot$ between 8 and 1000 μm, which is consistent with the $L_{\rm IR}$ derived using the method of Kim et al. (1995). We note that the total luminosity is dominated by the cool component.

3.2. IRAS 01250+2832

The SED of IRAS 01250+2832 is shown in Fig. 4. It is difficult to explain the flat SED at wavelengths between 9 μm and 60 μm with normal spiral and elliptical galaxy models (Silva et al. 1998). The spiral and elliptical galaxy templates do not have strong enough infrared emission. It is difficult to explain the global SED with starburst galaxy templates such as M 82 and Arp 220 that have a strong excess in the FIR. Here, we assume that the host galaxy is dominated by an old stellar population (13 Gyr; Silva et al. 1998) based on the strong $D_n(4000)$ index.

When we also fit the AKARI NIR spectrum using Eq. (2) and the elliptical galaxy template, we need to introduce a blackbody component of temperature of 510 ± 20 K in optically thick conditions as shown in Fig. 4b. Another blackbody component of 100 K is needed to explain the *IRAS* 60 μm flux. The higher fluxes of the model relative to those observed at 9 and 12 μm can be attributed to 9.7 μm silicate absorption, which is not included in this model. However, it is expected to be present based on the CO absorption measured at 4.75 μm. The conclusion that the SED needs two blackbody components does not change much even if we use spiral galaxy templates. The infrared luminosity $L_{\rm IR}$ is derived to be $9.1 \times 10^{10}\ L_\odot$, which is consistent with

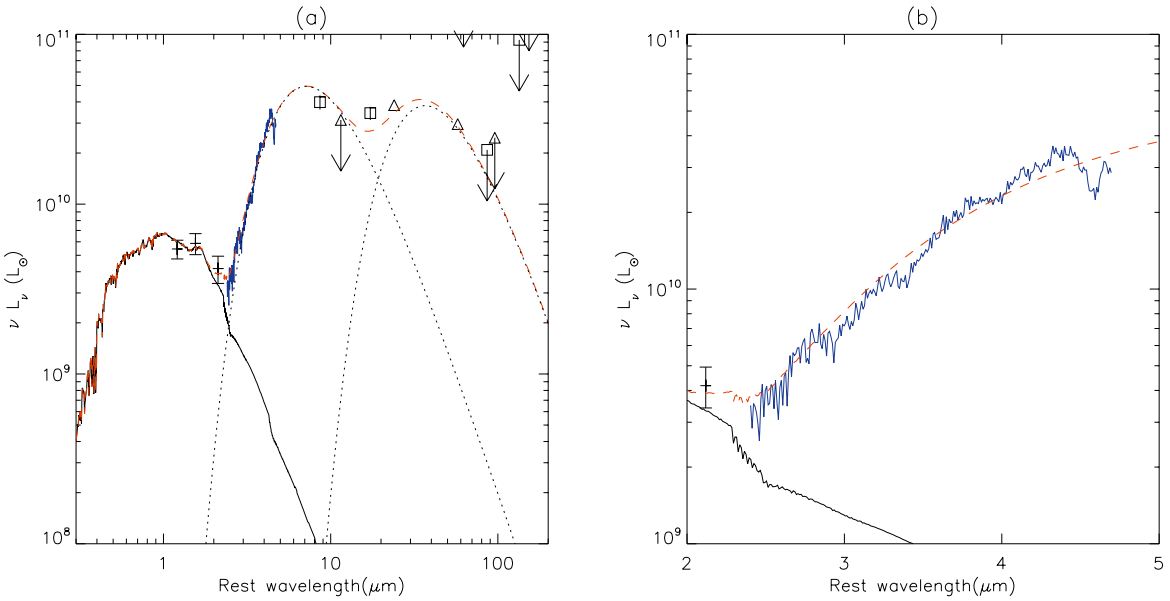

Fig. 4. Same as Fig. 4 except for IRAS 01250+2832. A model template of an elliptical galaxy (Silva et al. 1998) is used. Two blackbodies in this figure have temperatures of 510 K and 100 K.

1.0×10^{11} $L_\odot$ using the method of Kim et al. (1995). We note that the contribution at wavelengths longer than 60 μm to the total luminosity is expected to be small for IRAS 01250+2832.

While there are no signs of Hβ and [O III] emission lines in Fig. 2b, Hα and [N II] lines are clearly detected. The [N II]6584 Å emission line is stronger than Hα, suggesting that IRAS 01250+2832 is a low-ionization nuclear emission-line region (LINER) galaxy. However, the other indicators of LINERs, [O I]6300 Å and [S II]6716 Å+6731 Å emission lines, are not seen because of the weakness of the lines, relative to the stellar continuum. The 3σ upper limit to the Hβ flux is estimated to be 3.0×10^{-16} erg s^{-1} cm^{-2}. This upper limit is not useful to estimate the reddening from the Balmer ratio. Without applying any reddening correction, we calculate an Hα line luminosity of 4.7×10^5 $L_\odot$, which is comparable to that of low-luminosity AGNs (LLAGNs) found in the optical spectroscopic survey of nearby galaxies (Ho et al. 1997). A comparison with LLAGNs is discussed in Sect. 5.

4. Hot dust with $T_{\rm dust}$ ~ 500–600 K

As shown in Sect. 3, both galaxies show near-infrared continuum from hot dust with $T_{\rm dust}$ = 500–600 K, although they differ in other ways. The origin of the energy source heating this dust, however, remains unclear.

Fits indicate that the luminosity of this hot dust component is 2.7×10^{10} $L_\odot$ and 6.6×10^{10} $L_\odot$ for LEDA 84274 and IRAS 01250+2832, respectively. If we assume one single optically thick spherical emitting region, the size of the emitting regions would be 0.7 pc and 1.6 pc in diameter for LEDA 84274 and IRAS 01250+2832, respectively. One possibility is that we are observing an OB star cluster that has a huge luminosity of $L_{\rm IR} > 10^{10}$ $L_\odot$ in a compact volume of a cubic parsec, and that heats up the surrounding dust to >500 K. However, the relaxation time of the dynamically bound system can be estimated to be 10^6–10^7 years. Thus, this situation is unlikely to be observed.

A more likely possibility is that the object is a compact central supermassive black hole surrounded by a hot accretion disk. However, no optical spectrum shows any evidence of the hard photons produced by an AGN. The various emission-line ratios of LEDA 84274 in the optical band show that it is an H II-region-like galaxy as Kim et al. (1995) concluded. IRAS 01250+2832 shows no emission lines except for Hα and [N II]. The weak- and non-detection of PAH 3.3 μm emission may support the presence of an obscured AGN. The equivalent widths of the PAH 3.3 μm emission feature are 0.018 μm and <0.003 μm for LEDA 84274 and IRAS 01250+2832, respectively. Observations of starbursts show equivalent widths of PAH 3.3 μm with an average value of 0.1 μm, and they are never smaller than 0.04 μm (Moorwood 1986; Imanishi et al. 2008). Thus the PAH equivalent width is diluted by strong featureless NIR continuum in IRAS 01250+2832 and completely overwhelmed in LEDA 84274.

The excess featureless near-IR continuum may alternatively represent multiple dusty OB star clusters, in which extraordinarily intense starbursts are occurring. This is seen in some interacting galaxies (Joseph et al. 1984; Joseph & Wright 1985). Hunt et al. (2002) also argue that the hot dust that produces the NIR color excess must be heated by massive stars. In this case, the weak PAH emission can be produced by the harder radiation fields of massive stars in these environments that can destroy PAHs (e.g. Beirão et al. 2006; Wu et al. 2006). From *Spitzer* imaging data of nearby irregular galaxies, excess emission at 4.5 μm from hot dust was found mostly in high-surface-brightness H II regions, implying that massive stars are the primary source of heating (Hunter et al. 2006). For IRAS 01250+2832, multiple dusty star clusters are less likely to be present, because most of dusty star clusters are surrounded by diffuse emission of PAHs as well as optical emission lines. IRAS 01250+2832 does not show any evidence for such activities.

If the assumption that the dust emission is optically thick is not correct, the NIR red continua of LEDA 84274 can be explained by a dust temperature of ~480–580 K and emissivity of $\lambda^{-\beta}$ with β = 1–2. In spiral galaxies that normally display the thermal emission of optically thin dust, Lu et al. (2003) detected non-stellar NIR excess continuum with a temperature of ~1000 K (β = 2) and concluded that the NIR excess continuum originates in the interstellar matter of the galaxies based

on the linear correlation between emission from aromatic carbon and the excess. In this case, the NIR excess has a luminosity of only a few percent of the FIR luminosity. However, the ratio of the NIR luminosity to the FIR luminosity is 0.15 and 0.75 for LEDA 84274 and IRAS 01250+2832, respectively. Thus, the emission from the hot dust in LEDA 84274 and IRAS 01250+2832 seems to be different from those of spiral galaxies.

We suspect that the hot dust associated with obscured AGNs. But the possibility of multiple dusty star clusters in both objects, especially LEDA 84274, cannot be ruled out. Observations at other wavelengths can resolve the question. In particular, X-ray observations can provide important information on the energy source, but both galaxies are not detected in the ROSAT all-sky survey faint source catalogue (an upper limit of 1.3×10^{-13} erg cm^{-2} in the 0.1−2.4 keV band; Voges et al. 2000). Hard X-ray observations will thus be important.

5. Discussion

As discussed in Sect. 4, the compact hot dust component that we found in LEDA 84274 and IRAS 01250+2832 is likely to surround an AGN that is heating it, even though other possibilities cannot be completely ruled out. In this section, we discuss these dusty AGNs.

The optical spectra display no strong emission lines (especially high-excitation ones) from narrow-line regions. Thus, no narrow-line region on a 10−1000 pc scale is evident in these galaxies. IRAS 01250+2832 has a low-ionization spectrum that is typical of LLAGNs, as discussed in Sect. 3.2. The low-ionization state spectrum in LLAGNs may be produced by black-hole accretion at a very low rate (with a bolometric luminosity of $L_{\rm bolo} < 4 \times 10^{10}\ L_{\odot}$, Ho 2008). However, LEDA 84274 and IRAS 01250+2832 have much higher luminosities of $L_{\rm IR} \gtrsim 1 \times 10^{11}\ L_{\odot}$ at infrared wavelengths than LLAGNs. Large optical extinction of the central engine is a plausible explanation of their optical spectra. These findings indicate that the AGNs are surrounded by a large amount of dust, so that ionizing UV radiation from the AGN is blocked along virtually all lines of sight. In ultra-luminous and luminous infrared galaxy cores, similar situations are sometimes seen (e.g. Imanishi et al. 2010).

Since the observed radiation from AGNs is often reprocessed and re-emitted at infrared wavelengths, the intrinsic SED is altered substantially. Wide spectral coverage is necessary to determine the Eddington ratio ($L_{\rm bolo}/L_{\rm Edd}$, or equivalently $L_{\rm bolo}/M_{\rm BH}$) (e.g. Peterson 1997). Although it is difficult to differentiate the AGN component from the overall SED, we estimate the black-hole mass by making the a simple assumption that the AGN luminosity is nearly equal to the luminosity from the 500−600 K dust. Assuming spherical accretion toward the black hole with a radiative efficiency of 0.1, the supermassive black hole mass from the luminosities of the hot dust is at least $8 \times 10^6\ M_{\odot}$ and $2 \times 10^7\ M_{\odot}$ for LEDA 84274 and IRAS 01250+2832, respectively. These do not differ significantly from the black hole masses estimated from the 9 μm luminosities using the bolometric correction evaluated using a Type2 QSO template in Polletta et al. (2007)[2]. Thus, we adopt the black hole mass estimates from the luminosities of the hot dust in the following discussion. If they have a higher radiative efficiency, the masses will be lower.

The masses of these host galaxies can be calculated to be $6 \times 10^9\ M_{\odot}$ and $4 \times 10^9\ M_{\odot}$ for LEDA 84274 and IRAS 01250+2832, respectively, using the 2MASS $K_{\rm S}$ photometry and the mass-to-luminosity ratio, $M_{\rm host}/L_{K_{\rm S}} \sim 1$ (Cole et al. 2001)[3]. The mass ratio of the black hole to the stellar component in the host galaxy is 1.3×10^{-3} and 5×10^{-3} for LEDA 84274 and IRAS 01250+2832. The results are consistent with the local relation between the mass of the central black hole and the stellar mass of the surrounding spheroid or the bulge in nearby galaxies, $M_{\rm bh}/M_{\rm bulge} = 1.4 \times 10^{-3}$ (Häring & Rix 2004). The mass of both host galaxies is relatively low, i.e., $6 \times 10^9\ M_{\odot}$ and $4 \times 10^9\ M_{\odot}$, for LEDA 84274 and IRAS 01250+2832, respectively. Large samples of AGNs from the Sloan Digital Sky Survey have host galaxy masses of $\log M_{\rm gal} = 9.5$−12 with $D_{\rm n}(4000) = 1.2$−2.2 (Kauffman et al. 2003). Our sample with $M_{\rm host} = 4$−$6 \times 10^9\ M_{\odot}$ and $D_{\rm n}(4000) = 1.1$−1.6 seems to be the least massive population that may harbor an AGN.

6. Summary

By combining data from the AKARI MIR All-Sky Survey and NIR spectroscopy, we have discovered two luminous infrared galaxies at $z \sim 0.04$ that have hot dust with a temperature of $\gtrsim$500 K. The hot dust is likely to be associated with AGNs, but the possibility that the hot dust is heated by multiple dusty star clusters of massive stars cannot be ruled out by our current data. If they are AGNs, their emission must be buried, because present AGN signatures are seen only in the NIR and MIR, not in the optical. If they have AGNs, the estimates of the black hole masses of ~ 8−$20 \times 10^7\ M_{\odot}$, and the host galaxy masses of ~ 4−$6 \times 10^9\ M_{\odot}$ also indicate that the population is less massive than optically selected AGNs (Kauffman et al. 2003). These objects were missed in previous surveys, demonstrating the power of AKARI MIR All-Sky Surveys to obtain a more complete view of the entire AGN population.

We have initiated a long-standing program to study AGNs detected from the AKARI MIR All-Sky Survey. Multiwavelength observations will provide larger samples of buried AGN candidates that are similar to those we present in this paper, examples of which we plan to present in the near future.

Acknowledgements. The authors thank the anonymous referee for constructive comments that helped to improve this paper. This research is based on observations with AKARI, a JAXA project with the participation of ESA. This research also makes use of data products from the Two Micron All Sky Survey, which is a joint project of the University of Massachusetts and the Infrared Processing and Analysis Center/California Institute of Technology, funded by the National Aeronautics and Space Administration and the National Science Foundation. SO is supported by the a Grand-in-Aid for Scientific Research from the Japan Society for the Promotion of Science (No. 22740134). DI is supported by the Nagoya University Global COE Program "Quest for Fundamental Principles in the Universe" from the Ministry of Education, Culture, Sports, Science, and Technology of Japan.

References

Alonso-Herrero, A., Pérez-González, P. G., Alexander, D. M., et al. 2006, ApJ, 640, 167
Balogh, M. L., Morris, S. L., Yee, H. K. C., Carlberg, R. G., & Ellingson, E. 1999, ApJ, 527, 54
Beirão, P., Brandl, B. R., Devost, D., et al. 2006, ApJ, 643, L1

[2] The hot dust luminosities estimated from the 500−600 K blackbody are 30 percent higher and 4 percent lower than those estimated from the bolometric correction, for LEDA 84274 and IRAS 01250+2832, respectively.

[3] In Cole et al. (2001), mean stellar mass-to-light ratios are estimated to be 0.73 and 1.32 $M_{\odot}/L_{\odot}$ for the Kennicutt and the Salpeter initial mass functions, respectively.

Bruzual, A. G. 1983, ApJ, 273, 105
Cole, S., Norberg, P., Baugh, C. M., et al. 2001, MNRAS, 326, 255
Condon, J. J., Cotton, W. D., Greisen, E. W., et al. 1998, AJ, 115, 1693
Cowie, L. L., Songaila, A., Hu, E. M., & Cohen, J. G. 1996, AJ, 112, 839
Fabian, A. C., & Iwasawa, K. 1999, MNRAS, 303, L34
Haas, M., Klaas, U., Müller, S. A. H., et al. 2003, A&A, 402, 87
Häring, N., & Rix, H.-W. 2004, ApJ, 604, L89
Heckman, T. M., Kauffmann, G., Brinchmann, J., et al. 2004, ApJ, 613, 109
Helou, G., Soifer, B. T., & Rowan-Robinson, M. 1985, ApJ, 298, L7
Ho, L. C. 2008, ARA&A, 46, 475
Ho, L. C., Filippenko, A. V., & Sargent, W. L. W. 1997, ApJ, 487, 568
Hunt, L. K., Giovanardi, C., & Helou, G. 2002, A&A, 394, 873
Hunter, D. A., Elmegreen, B. G., & Martin, E. 2006, AJ, 132, 801
Imanishi, M., Nakagawa, T., Ohyama, Y., et al. 2008, PASJ, 60, 489
Imanishi, M., Maiolino, R., & Nakagawa, T. 2010, ApJ, 709, 801
Ishihara, D., Acke, B., Verhoelst, T., et al. 2010, A&A, 514, A1
Joseph, R. D., & Wright, G. S. 1985, MNRAS, 214, 87
Joseph, R. D., Meikle, W. P. S., Robertson, N. A., & Wright, G. S. 1984, MNRAS, 209, 111
Kauffmann, G., Heckman, T. M., Tremonti, C., et al. 2003, MNRAS, 346, 1055
Kennicutt, R. C., Jr. 1998, ARA&A, 36, 189
Kim, D.-C., Sanders, D. B., Veilleux, S., Mazzarella, J. M., & Soifer, B. T. 1995, ApJS, 98, 129
Lacy, M., Storrie-Lombardi, L. J., Sajina, A., et al. 2004, ApJS, 154, 166
Leipski, C., Haas, M., Meusinger, H., et al. 2005, A&A, 440, L5
Leipski, C., Haas, M., Meusinger, H., et al. 2007, A&A, 464, 895
Lu, N., Helou, G., Werner, M. W., et al. 2003, ApJ, 588, 199
Lutz, D., Spoon, H. W. W., Rigopoulou, D., Moorwood, A. F. M., & Genzel, R. 1998, ApJ, 505, L103
Maiolino, R., Salvati, M., Bassani, L., et al. 1998, A&A, 338, 781
Malizia, A., Stephen, J. B., Bassani, L., et al. 2009, MNRAS, 399, 944
Moorwood, A. F. M. 1986, A&A, 166, 4
Moshir, M., Kopman, G., & Conrow, T. A. O. 1992, Pasadena: Infrared Processing and Analysis Center, California Institute of Technology, ed. M. Moshir, G. Kopman, T. A. O. Conrow
Mouri, H., Kawara, K., Taniguchi, Y., & Nishida, M. 1990, ApJ, 356, L39
Murakami, H., Baba, H., Barthel, P., et al. 2007, PASJ, 59, 369
Ohyama, Y., Onaka, T., Matsuhara, H., et al. 2007, PASJ, 59, 411
Onaka, T., Matsuhara, H., Wada, T., et al. 2007, PASJ, 59, 401
Osterbrock, D. E., & Ferland, G. J. 2006, Astrophysics of gaseous nebulae and active galactic nuclei, ed. D. E. Osterbrock, & G. J. Ferland (Sausalito, CA: University Science Books)
Peterson, B. M. 1997, An Introduction to Active Galactic Nuclei (Cambridge: Cambridge Univ. Press)
Polletta, M. D. C., Wilkes, B. J., Siana, B., et al. 2006, ApJ, 642, 673
Polletta, M., Tajer, M., Maraschi, L., et al. 2007, ApJ, 663, 81
Risaliti, G., Maiolino, R., & Salvati, M. 1999, ApJ, 522, 157
Rush, B., Malkan, M. A., & Spinoglio, L. 1993, ApJS, 89, 1
Rush, B., Malkan, M. A., & Edelson, R. 1996, ApJ, 473, 130
Sanders, D. B., & Mirabel, I. F. 1996, ARA&A, 34, 749
Sanders, D. B., Soifer, B. T., Elias, J. H., et al. 1988, ApJ, 325, 74
Silva, L., Granato, G. L., Bressan, A., & Danese, L. 1998, ApJ, 509, 103
Skrutskie, M. F., Cutri, R. M., Stiening, R., et al. 2006, AJ, 131, 1163
Spinoglio, L., & Malkan, M. A. 1989, ApJ, 342, 83
Takagi, T., Vansevicius, V., & Arimoto, N. 2003, PASJ, 55, 385
Ueda, Y., Akiyama, M., Ohta, K., & Miyaji, T. 2003, ApJ, 598, 886
Veilleux, S., Kim, D.-C., Sanders, D. B., Mazzarella, J. M., & Soifer, B. T. 1995, ApJS, 98, 171
Voges, W., Aschenbach, B., Boller, T., et al. 2000, IAU Circ., 7432, 1
Weingartner, J. C., & Draine, B. T. 2001, ApJ, 548, 296
Wu, Y., Charmandaris, V., Hao, L., et al. 2006, ApJ, 639, 157
Yamamura, I., Makiuti, S., Ikeda, N., et al. 2009, ASP Conf. Ser., 418, 3
Yamamura, I., Makiuti, S., Ikeda, N., et al. 2010, AKARI/FIS All-Sky Survey Bright Source Catalogue Version 1.0 Release Note